ACS OMEGA

Open Access

http://pubs.acs.org/journal/acsodf

Article

Tandem Hydroperoxyl–Alkylperoxyl Radical Quenching by an Engineered Nanoporous Cerium Oxide Nanoparticle Macrostructure (NCeONP): Toward Efficient Solid-State Autoxidation Inhibitors

Riccardo Amorati,* Yafang Guo, Bridgette Maria Budhlall, Carol Forance Barry, Dongmei Cao, and Siva Sai Ramana Kumar Challa*

Cite This: *ACS Omega* 2023, 8, 40174–40183

Read Online

ACCESS | Metrics & More | Article Recommendations | Supporting Information

ABSTRACT: The use of nanomaterials as inhibitors of the autoxidation of organic materials is attracting tremendous interest in petrochemistry, food storage, and biomedical applications. Metal oxide materials and CeO_2 in particular represent one of the most investigated inorganic materials with promising radical trapping and antioxidant abilities. However, despite the importance, examples of the CeO_2 material's ability to retard the autoxidation of organic substrates are still lacking, together with a plausible chemical mechanism for radical trapping. Herein, we report the synthesis of a new CeO_2-derived nanoporous material (NCeONP) with excellent autoxidation inhibiting properties due to its ability to catalyze the cross-dismutation of alkyl peroxyl ($ROO^\bullet$) and hydroperoxyl ($HOO^\bullet$) radicals, generated in the system by the addition of the pro-aromatic hydrocarbon γ-terpinene. The antioxidant ability of NCeONP is superior to that of other nanosized metal oxides, including TiO_2, ZnO, ZrO_2, and pristine CeO_2 nanoparticles. Studies of the reaction with a sacrificial reductant allowed us to propose a mechanism of inhibition consisting of H atom transfer from $HOO^\bullet$ to the metal oxides ($MO_x + HOO^\bullet \rightarrow MO_x{-}H^\bullet + O_2$), followed by the release of the H atom to an $ROO^\bullet$ radical ($MO_x{-}H^\bullet + ROO^\bullet \rightarrow MO_x + ROOH$). Besides identifying NCeONP as a promising material for developing effective antioxidants, our study provides the first evidence of a radical mechanism that can be exploited to develop novel solid-state autoxidation inhibitors.

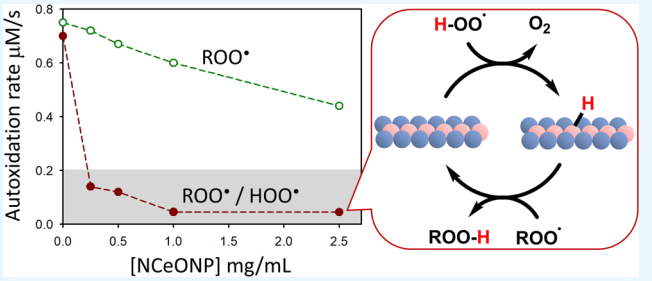

1. INTRODUCTION

Autoxidation of organic materials, that is, their spontaneous reaction with oxygen (O_2), represents a major hurdle in disparate fields ranging from petrochemistry to food storage and biomedical applications. In the last 70 years, many antioxidant strategies have been put forward. The first were based on the use of synthetic additives, including phenols, aromatic amines, sulfides, and phosphines.[1] More recently, natural inhibitors with food-grade or generally recognized as safe (GRAS) status, especially for the applications linked to the food and pharmaceutical industries, have been "rediscovered".[2−5] In general, both synthetic and natural antioxidants can play different roles based on their mechanism. While primary antioxidants function essentially as free radical terminators (chain-breaking antioxidants), secondary antioxidants are more likely to be preventive antioxidants that function by retarding chain initiation. Natural antioxidants, however, often have lower activity and higher costs than synthetic systems.[6] Therefore, novel strategies to achieve the same potency must be implemented, for instance, by taking advantage of the synergy between different kinds of antioxidants.[4]

The use of nanomaterials with antioxidant properties (also called nanoantioxidants) is a recent breakthrough in this field. These nanomaterials merge control of the autoxidation reaction with the advantages typical of nanosized objects. Such antioxidant nanomaterials, be they organic or inorganic, exhibit intrinsic redox activity that is often associated with radical trapping and/or with superoxide dismutase-like and catalase-like activities.[7−10] Given the exceedingly fast reaction of alkyl radicals ($R^\bullet$) with O_2, peroxyl radicals are the most significant chain-carrying radicals of the autoxidation in biological membranes (i.e., lipid peroxidation) and in oxidizable materials in general (polymers, fats, and oils).[7] In order to have chain-breaking antioxidant properties, a given nanomaterial must quench peroxyl radicals ($ROO^\bullet$), by reducing them to hydroperoxides (Scheme 1) by a formal

Received: May 24, 2023
Accepted: October 5, 2023
Published: October 18, 2023

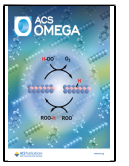

Scheme 1. Mechanism of Action of Nanoantioxidants for the Inhibition of Lipid Peroxidation[a]

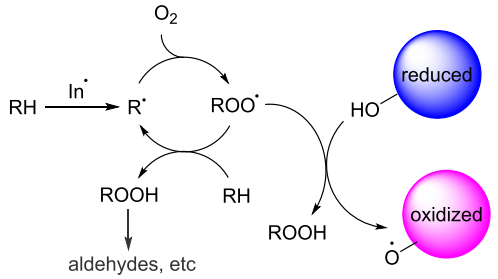

[a]The alkylperoxyl radicals that are the chain-carrying species of the oxidative chain are quenched by a H atom transfer.

hydrogen atom transfer. The reaction mechanism may consist of H atom donation from H atom-donating groups present on the surface or, in protic solvents such as water, by a proton-coupled electron transfer, in which the electron is donated by the nanomaterial, and the proton is provided by the solvent.[7]

Cerium oxide (CeO_2) nanoparticles represent one of the most popular metal oxide nanomaterials having antioxidant properties in cells and tissues.[11−13] Their activity is deeply connected to the ability to decompose hydrogen peroxide (H_2O_2) by cycling the surface cerium ions between the Ce^{3+}/Ce^{4+} redox states.[11,14] Despite the importance of CeO_2 nanomaterials, the studies of their reactions with alkyl peroxyl ($ROO^•$) radicals are scarce and contradictory. Lee et al.[15] reported that 3.8 nm CeO_2 nanoparticles capped with alkylamine/oleic acid were able to trap hydrosoluble radicals produced by 2,2′-azobis(2-amidinopropane) dihydrochloride (AAPH) at pH 7 and had a higher antioxidant capacity (i.e., trapped more radicals) than a water-soluble derivative of vitamin E, Trolox, in the oxygen radical absorbing capacity (ORAC) assay. In contrast, investigations of the reaction of luminol or lucigenin with alkyl peroxyl radicals (from AAPH) or superoxide ($O_2^{•−}$, from xanthine/xanthine oxidase) in water at pH 7.4 showed that citrate-stabilized 3 nm CeO_2 nanoparticles were much less active than Trolox and superoxide dismutase (SOD).[16] Moreover, there is no information regarding the ability of CeO_2 to stop lipid peroxidation or to react with oxygen-centered radicals in nonaqueous solvents.

Mayer and co-workers have recently developed the conceptual framework for H atom donation from nanosized metal oxides.[17−21] Reducible oxide nanoparticles, including CeO_2 and titanium dioxide (TiO_2), may be reduced by sacrificial hydrogen (H) atom donors like hydroquinones. Thereafter they can donate the H atom to stable radicals such as 2,2-diphenylpycrylhydrazyl ($DPPH^•$) or 2,2,6,6-tertamethylpyridinoxyl (TEMPO). Kinetic and thermochemical experiments, as well as quantum mechanical calculations, clearly show that it is possible to describe H atom donation by nanomaterials in terms of "bond dissociation energy" of labile O−H groups present on the surface, thereby applying concepts familiar to the chemistry of "molecular" free radicals and antioxidants. Regarding the nature of the surface H atom donors, it is proposed that they are most likely represented by hydroxy (OH) groups present on the surface of reducible oxides, where the proton is linked to a surface O atom (Scheme 2). At the same time, a reduced metal atom hosts the electron.[20]

Scheme 2. Nature of the Groups Able to Exchange H Atoms on the Surface of Reducible Ions, Such as Ce^{3+}/Ce^{4+}, Where XH and $Y^•$ Represent a Sacrificial H Atom Donor and a Radical Able to Abstract a H Atom, Respectively

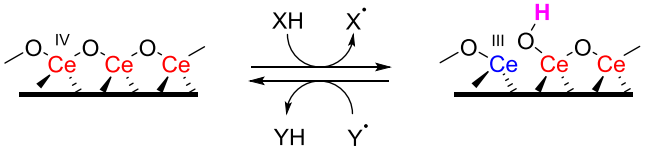

We describe in this work the reactivity with $ROO^•$ radicals of engineered nanoporous cerium oxide nanoparticle macrostructures (NCeONPs), whose synthesis and interesting redox properties have been recently discovered by some of us.[22] In order to establish the potential use of NCeONPs as an antioxidant in organic materials like plastics and oils on sound mechanistic grounds, we investigate NCeONPs' capacity to inhibit the autoxidation of organic substrates. For comparison, we also considered commercial CeO_2, TiO_2 anatase, TiO_2 rutile, zinc oxide (ZnO), and zirconium oxide (ZrO_2) nanoparticles as they play an important role in many industrial applications and can exhibit metallic, semiconductor, or insulator characteristics.[23] Besides the ability to trap $ROO^•$ radicals, we investigated the capability of these oxides to act as catalytic antioxidants by catalyzing the cross-dismutation of $ROO^•$ and hydroperoxyl ($HOO^•$) radicals (i.e., the protonated form of superoxide, $O_2^{•−}$). There is increasing evidence that $ROO^•$ and $HOO^•$ coexist during the autoxidation of substrates having alcohol, amine, amide, and alkene functional groups;[24] the interplay between these two radicals positively influences the antioxidant activity duration of α-tocopherol (α-TOH, see Scheme 3A)[25] and of aromatic amines as inhibitors of ferroptosis[26] with huge implications in the food and biomedical fields. Moreover, redox-active molecules (such as nitroxides[27,28] and quinones[29]) and biomaterials like polydopamine[30] display antioxidant activity through catalyzing $ROO^•$ and $HOO^•$ cross-dismutation (see Scheme 3).

The study of the inhibited autoxidation of a reference organic substrate showed that none of these materials had a direct antioxidant effect due to $ROO^•$ quenching. Still, some oxides, especially NCeONPs, behaved as oxidation inhibitors in the presence of a synergic coantioxidant able to generate mixed $ROO^•$ and $HOO^•$ radicals. These results are explained in the framework of the abovementioned theory of H atom transfer from metal oxides, and the implication for developing solid-state antioxidants is discussed.

2. MATERIALS AND METHODS

2.1. Materials. All chemicals (styrene, γ-terpinene, 2,2,5,7,8-pentamethyl-6-chromanol, *tert*-butylhydroquinone, *tert*-butylbenzoquinone, and azobis(isobutyronitrile) (AIBN)) were commercially available (Merk, Milan, Italy) and were used as received unless otherwise specified. γ-Terpinene and styrene were purified by percolating them twice on basic alumina microcolumns to remove stabilizers. AIBN was recrystallized from methanol. Solvents including acetonitrile (MeCN) were HPLC-grade and used without further purification. The metal oxide nanoparticles were obtained from Sigma-Aldrich, Skyspring Nano, and Nanoshell. TEM characterization is reported in Figure S1.

The nanoporous cerium oxide nanoparticle macrostructure (NCeONP) was prepared by controlled heating, under an

https://doi.org/10.1021/acsomega.3c03654
ACS Omega 2023, 8, 40174−40183

Scheme 3. Examples of (A) α-Tocopherol Regeneration by HOO$^{\bullet}$ and Catalytic Cross-Dismutation of ROO$^{\bullet}$ and HOO$^{\bullet}$ Radicals by (B) Nitroxides and (C) Quinones

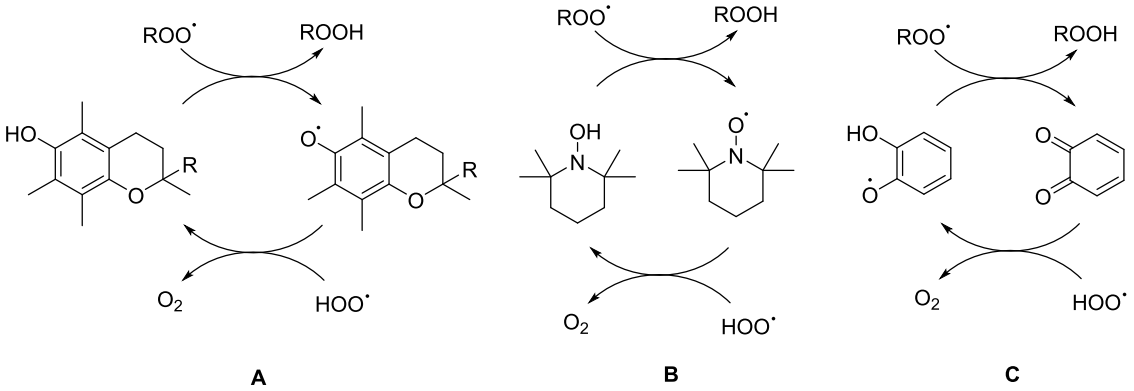

inert atmosphere, of CeO_2 nanoparticles to obtain controlled porosity and macrostructure.[22] Briefly, the commercially obtained cerium oxide nanoparticles were placed in a furnace; after the furnace was degassed and filled with nitrogen (N_2) gas, the particles were heated for 2 h to obtain the nanoporous cerium oxide nanoparticle macrostructure (NCeONP). The particles' pore width, surface area, and pore volume were controlled by the temperature at which the particles were heated.

2.2. Material Characterization. The particle sizes and size distribution of the nanoparticles were investigated by both transmission electron microscopy (TEM) and scanning electron microscopy (SEM). TEM was conducted on a Phillips EM400T instrument. The nanoparticles were prepared on carbon-coated TEM grids of 300 mesh size and dried under vacuum for 24 h before imaging.

Field-emission scanning electron microscopy (FE-SEM) was performed to determine the morphology of the nanoparticles. The FE-SEM (Model JEOL JSM 7401F) instrument is equipped with a cold-cathode tip field-emission gun, 1.0 nm resolution at 15 kV accelerating voltage, 0.1−30 kV accelerating voltage range, and 25×−1,000,000× magnification range. The detectors used were one chamber-mounted Everhart−Thornley-type secondary electron detector, one semi-in-lens secondary electron detector with r-filter and secondary electron signal enhancer, and one pneumatically retractable solid-state backscattered electron detector for topographical and compositional image contrast.

To determine the identity and chemical composition of the nanoparticles, X-ray microanalysis with energy-dispersive spectroscopy (EDS) was carried out on a ThermoFisher Helio G4 Xe PFIB/SEM dual beam system integrated with an Oxford EDS detector.

Both SEM imaging and EDS analysis were performed using the powder samples that were fixed on a SEM stub with double-sided carbon tape and coated with a thin layer of platinum before they were imaged with SEM and analyzed with EDS (Figure S2).

A dynamic light scattering (DLS) technique was also used to measure the particle size of the nanoparticles using a Malvern Zetasizer Nano-ZS instrument equipped with a 633 nm laser and a 173° scattering angle with noninvasive backscatter technology.

The pore volume, pore width, and specific surface area (SSABET) were measured from the dried nanoparticle samples with nitrogen sorption measurements (TriStar 3000, Micromeritics Inc.) and mercury intrusion porosimetry (MIP). The specific surface area was calculated according to BET theory. The pore volume and width were taken as the total adsorbed amount at a relative pressure of $p/p_o = 0.9$.

X-ray diffraction (XRD) of the nanoparticles was carried out on a Malvern Panalytical Empyrean X-ray diffractometer. The copper X-ray source operated at 45 kV with a beam current of 40 mA and a Pixcel3D detector recorded the spectra at a step size of 0.026°, dwell time of 116.8 s, and scanning 2θ range of 20−90°.

The XPS measurements were performed using a ScientaOmicron ESCA 2SR X-ray photoelectron spectroscopy system equipped with a flood source charge neutralizer. The powder samples were gently pressed into a thin pellet on double-sided carbon tape on the sample stage and then loaded into the loadlock chamber and pumped until the vacuum was below 5×10^{-7} mBar before they were transferred into the sample analysis chamber.[31,32] All analyses were carried out with a Mono Al Kα X-ray source (1486.6 eV) at the power of 300 W; and the pressure in the analysis chamber was maintained below 5×10^{-9} mBar. A wide region survey scan and high-resolution core-level scans of all elements were recorded and calibrated with the C 1s 284.8 eV as the reference peak. The core-level spectra were deconvoluted to obtain chemical state information.

2.3. Autoxidation Experiments. Autoxidation was performed in a two-channel oxygen uptake apparatus based on a Validyne DP-15 differential pressure transducer. The peroxyl radical-trapping activity was evaluated by studying the inhibition of thermally initiated autoxidation of styrene in acetonitrile (MeCN). In a typical experiment, a precisely weighed aliquot of the nanoparticles (1−2 mg) was dispersed by sonication in 1 mL of acetonitrile; then, the oxidizable substrate (styrene and γ-terpinene), 2 mL of an AIBN solution in acetonitrile (MeCN, 0.05 M), and MeCN were added to reach an overall volume of 4 mL. The sample was equilibrated with an identical reference solution containing an excess of the α-tocopherol analogue 2,2,5,7,8-pentamethyl-6-chromanol. The oxygen consumption in the sample was measured after calibration of the apparatus from the differential pressure recorded with time between the two channels.[25,27,29] The nanopowders were dispersed by stirring with a magnetic stir bar throughout the experiment. A short initial period with fast O_2 consumption was observed in experiments with low metal oxide concentrations. In these cases, the O_2 consumption slope was measured at the end of this initial period.

https://doi.org/10.1021/acsomega.3c03654
ACS Omega 2023, 8, 40174−40183

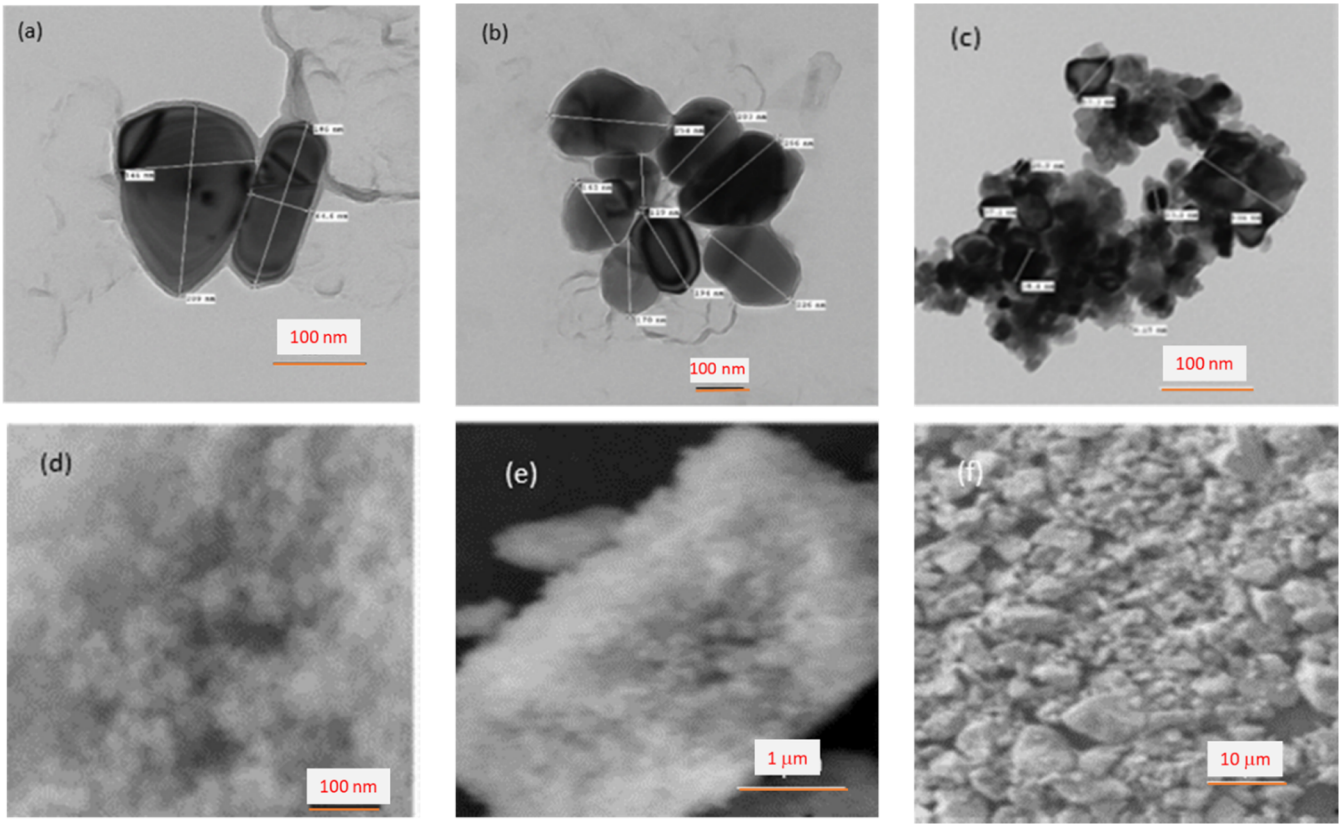

Figure 1. TEM (a–c) and SEM (d–f) images of (a–c) NCeONP particles and (d–f) their nonporous macrostructure.

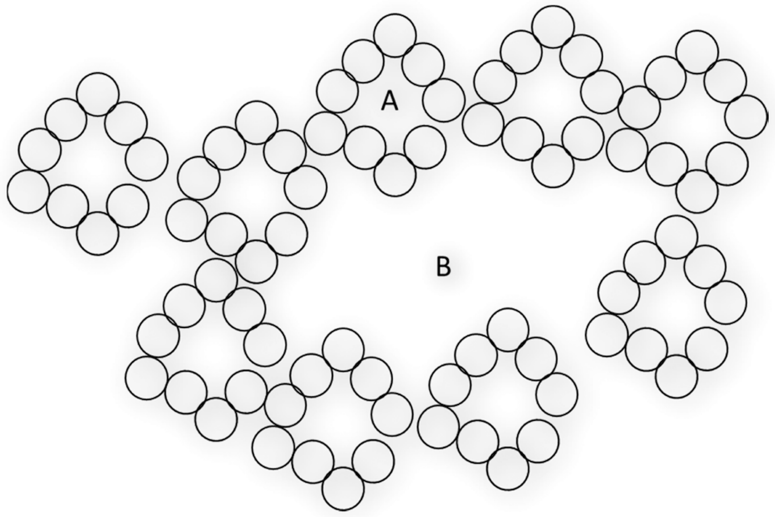

Figure 2. Schematic of the nanoporous cerium oxide macrostructure with different pore sizes: (A) nanopore and (B) microporous macrostructures.

2.4. Spectrophotometric Study of the Reaction with *tert*-Butylhydroquinone. The reaction of the various oxides with *tert*-butylhydroquinone (QH_2) was studied by ultraviolet–visible (UV–vis) spectroscopy in acetonitrile solutions under N_2, to avoid the oxidation of QH_2 by atmospheric O_2. The oxides (2 mg) were dispersed in 2 mL of MeCN; then, O_2 was removed by thoroughly N_2 bubbling and 200 μL of a deaerated 10 mM solution of QH_2 was injected through a rubber septum. After 4 h, a 500 μL portion of the supernatant obtained after decantation was diluted with 2 mL of MeCN and the absorbance was measured using a spectrophotometer in a 1 cm glass cuvette. Solutions of QH_2 and of *tert*-butylbenzoquinone (Q) in MeCN were used as references.

3. RESULTS AND DISCUSSION

3.1. Material Characterization. Both TEM and SEM images were used to characterize the nanoporous cerium oxide nanoparticles. As shown in Figures 1a–1c and S3–S4, the NCeONPs had a large particle size distribution, ranging from nanoscale to microns. The TEM images also showed individual CeO_2 nanoparticles as well as clusters of nanoparticles with nanoporosity (Figure 1b,1c). The particles were irregular in

https://doi.org/10.1021/acsomega.3c03654
ACS Omega 2023, 8, 40174–40183

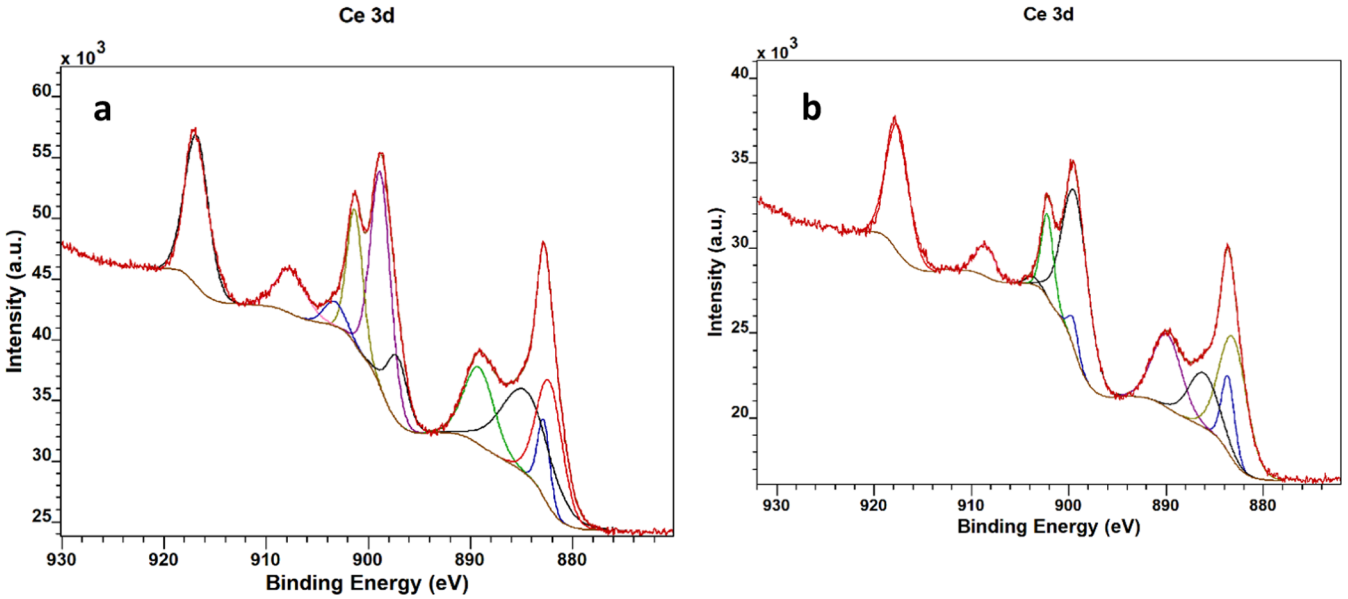

Figure 3. XPS spectra of Ce 3d of (a) NCeONPs and (b) commercial CeO_2 nanoparticles.

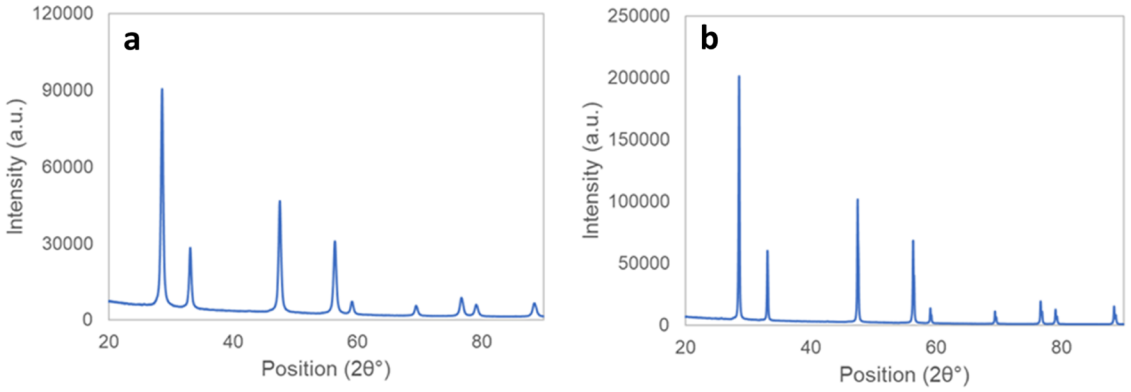

Figure 4. XRD patterns for (a) NCeONPs and (b) commercial CeO_2 nanoparticles.

Scheme 4. Generation of Hydroperoxyl Radicals (HOO•) by γ-Terpinene (γ-T) Forming *para*-Cymene (*p*-Cy)

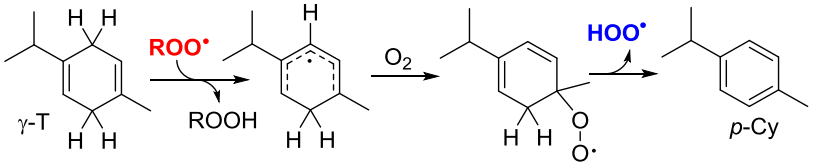

shape, i.e., mis-shaped ovoids, spheres, and cylinders. Figure 1d−1f also indicates that the irregularly shaped particles were not aggregated and had nanoscale pores on their surface. After suspending NCeONPs in water, DLS measurements of the supernatant (Figure S5) showed a bimodal particle size distribution with one small peak centered around 10 nm and the other at about 180 nm due to individual CeO_2 and small aggregates, respectively. Density functional theory (DFT)-based porosity and surface area measurements (based on N_2 adsorption) indicated that the surface area was 29.285 m^2/g and the pore width and pore volume were 10.7 nm and 0.073 cm^3/g, respectively (Figures S6 and S7). In contrast, mercury intrusion porosimetry, which measures larger pores, showed the presence of pore widths of 0.98 μm. Based on these characterization data and analyses, the nanoporous cerium oxide nanoparticle macrostructures (NCeONPs) are formed by the coalescence of CeO_2 nanoparticles to form larger particles (Figure 1a,b) that aggregate generating small and large pores. Therefore, the NCeONP has a binary size distribution with respect to both its macrostructure diameter (A) and macrostructure pore diameter (B); this structure is schematically shown in Figure 2.

The XPS spectra of Ce 3d of the NCeONP and cerium oxide nanoparticles (Figures 3, S8 and S9) showed a typical feature of the Ce(IV) spectrum; both had a peak at around 918 eV, which was absent from the spectrum of Ce 3d of Ce(III).[31,32] With both materials, the positions of Ce 3d 5/2 peaks were about 882 eV, which further confirmed that Ce in the nanoparticles was mostly in the Ce(IV) oxidation state.

The XRD patterns of NCeONPs and CeO_2 nanoparticles are presented in Figure 4. Both patterns are indexed to a cubic crystal structure. The crystal size calculated using the Scherrer

https://doi.org/10.1021/acsomega.3c03654
ACS Omega 2023, 8, 40174−40183

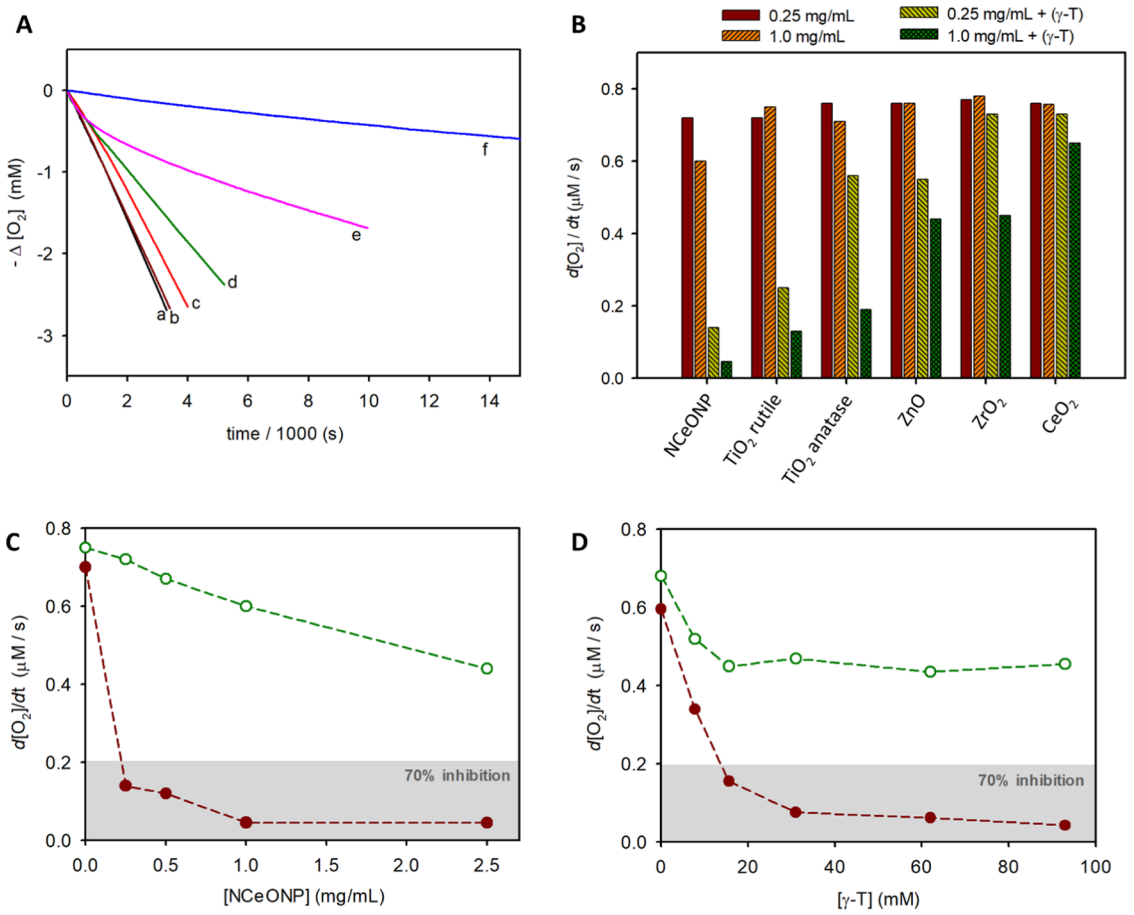

Figure 5. Results from the O_2 consumption measured during the autoxidation of styrene (2.2 M) initiated by AIBN (25 mM) at 30 °C in MeCN. (A) O_2 consumption traces (a) without inhibitors or in the presence of (b) NCeONP (0.25 mg/mL), (c) γ-T (16 mM), (d) NCeONP (1.0 mg/mL), (e) NCeONP (0.25 mg/mL + γ-T 16 mM), and (f) NCeONP (1.0 mg/mL + γ-T 16 mM). (B) Rate of O_2 consumption in the presence of two different concentrations of the metal oxides, with or without γ-T. (C) Rate of O_2 consumption with increasing NCeONP in the absence (○) or in the presence (●) of γ-T (16 mM). (D) Rate of O_2 consumption with increasing γ-T in the absence (○) or in the presence (●) of NCeONP (0.25 mg/mL).

equation was about 49 nm for the NCeONPs and approximately 107 nm for the CeO_2 nanoparticles.

3.2. Antioxidant Activity. The antioxidant activity was studied by measuring the ability to slow the consumption of the O_2 of the autoxidation of styrene, a reference oxidizable substrate; this reaction was initiated by the thermal decomposition of azobis(isobutyronitrile) (AIBN) at 30 °C in acetonitrile (MeCN). Styrene autoxidation follows the typical mechanism of the autoxidation of biologically relevant organic compounds, consisting of the initiation, propagation, and termination steps, which involve carbon ($R^•$)- and oxygen-centered peroxyl (ROO) radicals (Scheme 1).[1,2] The addition of small amounts of γ-terpinene (γ-T) generates $HOO^•$ radicals in the system through the cascade reactions illustrated in Scheme 4.[24] Typical styrene/γ-T ratios were 1:0.01 vol/vol, corresponding to 16 mM γ-T.

Figure 5A presents an example of the O_2 consumption results during the AIBN-initiated autoxidation of styrene or of a mixture of styrene and γ-T, either in the absence or in the presence of the various metal oxides. Trials were performed on newly synthesized NCeONP and on commercial metal oxide nanoparticles including TiO_2 anatase, TiO_2 rutile, ZnO, ZrO_2, and CeO_2 NPs at two representative concentrations (0.25 and 1 mg/mL). In the absence of antioxidants, O_2 consumption was fast and linear both in the case of styrene (trace a) and styrene/γ-T (trace c). Upon the addition of the metal oxides, no antioxidant effect was detected in the case of styrene alone (trace b); while in the case of the styrene/γ-T mixture, the O_2 consumption was reduced proportionally to the oxide concentration (traces d–f). The O_2 consumption slopes, reported in Figure 5B, showed that all metal oxides, when used alone, were poor inhibitors of the styrene autoxidation at both concentrations (first two red columns). This behavior was expected because they do not possess any reduced metal–OH groups that are able to react with $ROO^•$ radicals. In contrast, in the presence of styrene/γ-T, the metal oxides reduced O_2 consumption in a concentration-dependent manner (second two columns) and so exhibited good antioxidant activity. The activity decreased with the nanoparticles in the order of NCeONP > TiO_2 rutile > TiO_2 anatase > ZnO > ZrO_2 > CeO_2.

Further tests were conducted on the best material, NCeONP, to better understand its activity. Figure 5C,D shows the results of changing the concentrations of NCeONP and γ-T, respectively. Interestingly, even at low concentrations of NCeONP and γ-T (0.25 and 16 mM, respectively), a reduction of >70% of the initial rate of consumption of the O_2 was achieved. When the concentration of NCeONP was increased, some inhibition was observed even in the absence of γ-T (Figure 5C); this behavior is reasonably due to the traces

https://doi.org/10.1021/acsomega.3c03654
ACS Omega 2023, 8, 40174–40183

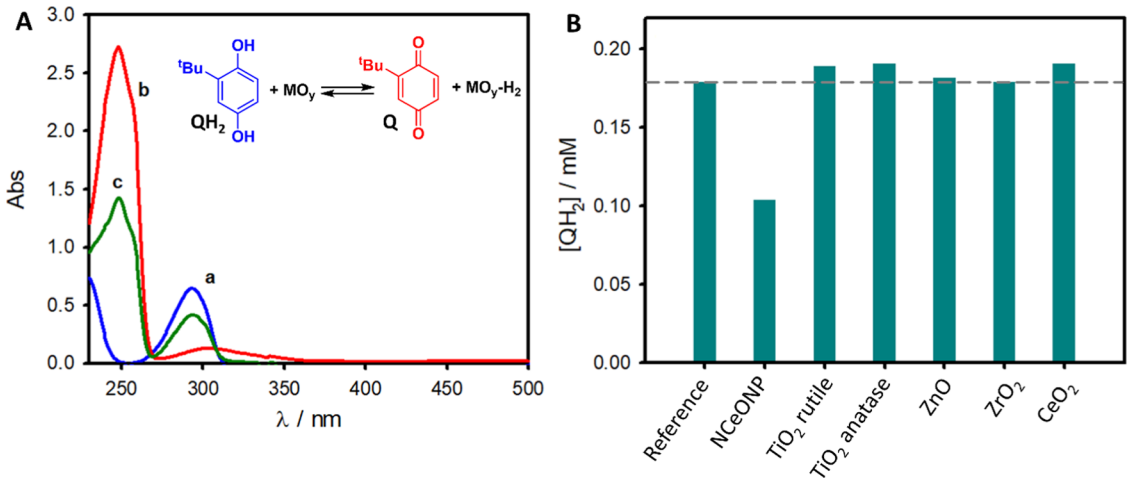

Figure 6. (A) UV−vis spectra of QH_2 (0.18 mM, trace (a)), Q (0.18 mM, trace (b)), and the mixture of QH_2/NCeONP (0.18 mM/0.9 mg/mL) after 4 h of reaction in MeCN under N_2 (trace c). (B) Concentration of QH_2 after 4 h of reaction with the nanopowders (0.9 mg/mL); the dashed line indicates the QH_2 initial concentration.

of HOO• produced during the autoxidation of styrene.[28] With 0.25 mg/mL NCeONP, increasing the γ-T concentration reduced the inhibition by 93% (Figure 5D). Additional trials determined that water and H_2O_2, a byproduct of γ-T autoxidation, were not able to increase the antioxidant activity (see Figures S9−S11). Moreover, there was no direct reaction between γ-T and NCeONP, i.e., without HOO• intermediation.

To clarify these results in the context of the catalytic cycle shown in Scheme 3, the ability of these materials to accept H atoms from an organic H atom donor was investigated. By following the procedure previously employed by Mayer and co-workers,[17] UV−vis spectroscopy was used to study the reaction of the various oxides with *tert*-butylhydroquinone (QH_2) in acetonitrile solutions under N_2. When QH_2 reduces the nanoparticles, it is oxidized to *tert*-butylquinone (Q) (as shown in Figure 6A) and has a UV−vis spectral signature different from QH_2. QH_2 has a typical absorption band at 293 nm, whereas Q has a strong absorption at 248 nm (Figure 6A, traces a and b). The UV−vis spectra measured after mixing QH_2 and NCeONP, presented in Figure 6A, trace c, clearly shows the consumption of QH_2 and the formation of Q. Besides, under these conditions, NCeONPs showed a weak absorption at 274 nm (Figure S13). Figure 6B shows the change in QH_2 concentration for all of the nanoparticles. Only in the presence of NCeONP was there a significant diminishing of the QH_2 concentration and the buildup of the corresponding quinone. Therefore, the NCeONP was the most oxidizing among the various oxides and the most prone to be reduced by sacrificial reductants.

The reactivity of the various metal oxides with QH_2 can be discussed by considering the difference in O−H bond dissociation-free energies (BDFE) between QH_2 and the O−H groups present on the surface of reduced oxides.[17] The mean BDFE of the two hydroxy groups in QH_2 is reported as 65 kcal/mol,[17] while the BDFE values of the reduced metal oxides OH groups (of which a possible structure is reported in Scheme 2), obtained by equilibration techniques with organic reductants or by theoretical calculations, are listed in Table 1[17,19−21,33−36] (no data are available for ZrO_2). It is readily apparent that CeO_2-derived nanomaterials have the largest BDFE of the surface OH groups among all metal oxides.

Table 1. Bond Dissociation-Free Energies (BDFE) for the OH Groups on the Surface of Reduced Metal Oxide Nanoparticles[a]

material	BDFE (kcal/mol)	refs
CeO_2	61.3 < BDFE < 74.3	17
	79.7[b,c]; 74.3[b,c]	33,35,36
TiO_2 rutile	<59	34
TiO_2 anatase	49.2	19
	39.4[a]	21
ZnO	<59	34
	61.2	20

[a]Unless otherwise stated, the values were obtained experimentally by equilibration with organic reductants or oxidants. Errors were estimated as ±0.3 kcal/mol. [b]Values from theoretical calculations. [c]BDFE values were estimated from the absorption enthalpy of atomic H•, calculated as 87.9 kcal/mol on 110 facets and 82.5 kcal/mol on 111 facets of CeO_2 (in gas phase). These values were transformed into BDFEs by using the conversion factor of −8.17 kcal/mol for the gas phase.[35,36]

Equilibration studies[17] showed that CeO_2 nanoparticles can display BDFE values as large as 74 kcal/mol, that is, 9 kcal/mol greater than that of the OH groups in QH_2, thus justifying the prompt reaction with QH_2. However, OH groups in partially reduced CeO_2 can display different BDFE values, depending on the particle size of the material.[17] Mayer and co-workers noted that the BDFE of the OH groups in partially reduced CeO_2 nanoparticles was lowered to 61.3 kcal/mol by increasing the concentration of Ce^{3+}.

XPS analysis of the NCeONP and CeO_2 nanoparticles, however, displayed similar compositions, with only little Ce^{3+} in both materials. It can be supposed that other effects play a role in the ease of reduction of CeO_2, such as the exposed facets in the crystals. It has been recently reported that sphere-, octahedron-, rod-, and cube-shaped CeO_2 nanomaterials have substantially different capabilities to form noncovalent interactions with a molecular probe (trimethylphosphine, Me_3P), as the effect of the different accessibility of surface Ce ions.[37] The crystal planes exposed by CeO_2 also have been indicated to be more important than the Ce^{3+}/Ce^{4+} ratio in determining the ability to trap HO• radicals[38] and to decompose H_2O_2.[39] The difference between the oxidizing

https://doi.org/10.1021/acsomega.3c03654
ACS Omega 2023, 8, 40174−40183

Scheme 5. General Mechanism Explaining the Synergic Antioxidant Effect of NCeONP and γ-terpinene: (A) Autoxidation of Organic Substrates, (B) Role Played by γ-Terpinene, and (C) Interplay between HOO• and Metal Oxides

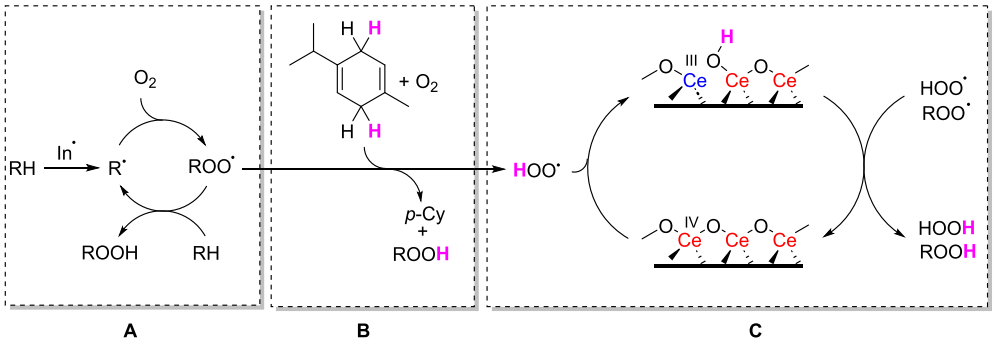

properties of NCeONP and CeO_2 nanoparticles can therefore be ascribed to the different crystalline structures of their surfaces. The thermal treatments used in NCeONP preparation enable control of these changes.

In analogy with what was observed in the case of nitroxides,[27] quinones,[29] and quinone-containing nanomaterials[30] and in the framework of the H atom transfer theory from metal oxides proposed by Mayer and co-workers,[17−21] the mechanism of antioxidant action observed herein can be explained by invoking the reactions reported in Scheme 5A−C. Scheme 5A is the typical reaction sequence of the autoxidation of organic substrates propagated by alkyl peroxyl radicals (ROO•). As ROO• is an oxidizing radical, it does not react with (oxidized) metal oxides, which therefore are unable to retard styrene autoxidation. Scheme 5B shows the crucial role played by γ-terpinene, i.e., transforming some chain-carrying ROO• radicals into HOO• radicals. Differently from ROO•, HOO• radicals have both oxidizing and reducing properties. In fact, HOO• radicals can abstract H atoms from organic substrates forming H_2O_2. Still, they also can easily donate a H atom since the BDFE of the H-OO• bond is as low as 51 kcal/mol (in water).[35] In Scheme 5C, the interplay between HOO• and metal oxides, in the specific example of CeO_2, is reported. Surface CeO_2 reacts with HOO• by accepting a H atom and forms a reduced species that, in turn, is oxidized back to CeO_2 by ROO• (or HOO•) radicals. In conclusion, CeO_2 works as a catalytic antioxidant, being able to accelerate HOO•/ROO• decomposition without being consumed during the reaction.

3.2.1. Can Metal Oxides Replace "Molecular" Chain-Breaking Antioxidants? Natural and synthetic antioxidants such as α-tocopherol, vitamin C, butylated hydroxytoluene (BHT), and diphenylamine act by donating a hydrogen atom to peroxyl radicals, which are the key chain-carrying species in autoxidation.[1] As demonstrated in this work, metal oxides cannot directly trap ROO• radicals because they do not possess surface hydrogen atoms or hydrogen atom equivalents (e^- and H^+) to be donated to ROO•. One may argue that metal oxides may be reduced by chemical methods, thus forming surface MO−H groups that should enable for H atom transfer to ROO• and might be used as a replacement for small-molecule antioxidants Unfortunately, reduced metal oxides have low BDFEs, so they are unstable under air during storage because they react with O_2 by reactions 1 and 2.

$$M^nO{-}H + O_2 \rightarrow M^{n+1}O + HOO^\bullet \quad (1)$$

$$M^nO{-}H + HOO^\bullet \rightarrow M^{n+1}O + H_2O_2 \quad (2)$$

Instability under air is a well-known major problem for antioxidants that limits the usefulness of molecules with very low BDFE(O−H).[40]

3.2.2. Which Possible Use for Metal Oxides as Antioxidants? As demonstrated in this work, the intermediate value of BDFE(O−H) of some metal oxides (especially NCeONP) suggests their use as catalytic antioxidants in the presence of a mixed ROO• and HOO•. Therefore, applications should focus on systems where the presence of both radicals is significant. The organic substrates that oxidize by forming ROO• and HOO• radicals includes primary and secondary alcohols, amines, amides, and alkenes.[24] Every time an alkyl peroxyl can undergo an easy 1,4-intramolecular H atom transfer, a fraction of it is converted to HOO•.[24] For example, it has been recently shown that the high-temperature oxidation of alkenes occurs with the formation of HOO•, which triggers the catalytic antioxidant effect of nitroxides.[28] Another characteristic of metal oxides that must be considered is the polarity and hydrophilicity of their surfaces, which reduce their dispersion in highly apolar samples (such as triacylglycerols) and their capability to interact with peroxyl radicals. Possible future research could improve this aspect by introducing surface capping agents that may tune and control the catalytic performance of the metal oxide.

4. CONCLUSIONS

We have shown herein that metal oxides are able to retard the autoxidation of an organic substrate in the presence of γ-terpinene, which acted as a coantioxidant. The best inhibitor was a novel nanoporous CeO_2-based material (NCeONP), obtained by the controlled heating under inert atmosphere conditions of CeO_2 nanoparticles. The inhibition mechanism was explained in terms of catalytic dismutation of the chain-carrying ROO• radicals with the HOO• radicals generated by γ-terpinene oxidation. Due to this mechanistic rationalization, it can be predicted that other easily oxidizable molecules, whose autoxidation proceeds via the formation of mixed ROO• and HOO• radicals, such as alkenes and amines, can be protected by NCeONP.[41] To the best of our knowledge, this is the first report of a solid-state antioxidant that is effective to retard the autoxidation of an organic compound. These findings are relevant for several technological applications, such as to reduce the oxidation of varnishes and paints, to avoid rubber degradation, and to protect oils and food from rancidity. An inorganic antioxidant for these applications is likely to be superior to organic antioxidants, as it is resistant to

https://doi.org/10.1021/acsomega.3c03654
ACS Omega 2023, 8, 40174−40183

degradation, may be incorporated into the packaging, and would not migrate into the protected material.

■ ASSOCIATED CONTENT

Supporting Information

The Supporting Information is available free of charge at https://pubs.acs.org/doi/10.1021/acsomega.3c03654.

Characterization of the materials (Figures S1−S9); diagram of O_2 uptake recording apparatus and O_2 consumption kinetics (Figures S10−S12); and UV−vis spectra of NCeONPs with and without H_2O_2 (Figure S13) (PDF)

■ AUTHOR INFORMATION

Corresponding Authors

Riccardo Amorati − *Department of Chemistry "G. Ciamician", University of Bologna, 40129 Bologna, Italy;* orcid.org/0000-0002-6417-9957; Email: riccardo.amorati@unibo.it

Siva Sai Ramana Kumar Challa − *Xheme, Inc.,, Newton, Massachusetts 02459, United States*; Email: kumar@xhemeinc.com

Authors

Yafang Guo − *Department of Chemistry "G. Ciamician", University of Bologna, 40129 Bologna, Italy*

Bridgette Maria Budhlall − *Department of Plastics Engineering, University of Massachusetts Lowell, Lowell, Massachusetts 01854, United States;* orcid.org/0000-0002-6096-6523

Carol Forance Barry − *Department of Plastics Engineering, University of Massachusetts Lowell, Lowell, Massachusetts 01854, United States*

Dongmei Cao − *Shared Instrumentation Facility, Louisiana State University, Baton Rouge, Louisiana 70809, United States*

Complete contact information is available at: https://pubs.acs.org/10.1021/acsomega.3c03654

Notes

The authors declare the following competing financial interest(s): SSRKC is employed by Xheme Inc, a for-profit organization, and both SSRKC & RA are co-inventors on a pending patent application.

■ ACKNOWLEDGMENTS

SSRKC gratefully acknowledges partial support for this research from the NSF-STTR Grant #Award Number (FAIN): 2037947. Dr Earl Ada is acknowledged for his help to characterize the NCeONP using TEM. Dr. Nagabhushana KS is acknowledged for help with porosity measurements.

■ REFERENCES

(1) Valgimigli, L.; Pratt, D. A. Antioxidants in Chemistry and Biology. *Encycl. Radicals Chem. Biol. Mater.* **2012**, DOI: 10.1002/9781119953678.rad055.

(2) Helberg, J.; Pratt, D. A. Autoxidation vs. Antioxidants − the Fight for Forever. *Chem. Soc. Rev.* **2021**, *50* (13), 7343−7358.

(3) Forman, H. J.; Zhang, H. Targeting Oxidative Stress in Disease: Promise and Limitations of Antioxidant Therapy. *Nat. Rev.* **2021**, *20*, 689−709.

(4) Amorati, R.; Valgimigli, L. Methods to Measure the Antioxidant Activity of Phytochemicals and Plant Extracts. *J. Agric. Food Chem.* **2018**, *66*, 3324−3329.

(5) Mollica, F.; Lucarini, M.; Passerini, C.; Carati, C.; Pavoni, S.; Bonoldi, L.; Amorati, R. Effect of Antioxidants on High-Temperature Stability of Renewable Bio-Oils Revealed by an Innovative Method for the Determination of Kinetic Parameters of Oxidative Reactions. *Antioxidants* **2020**, *9*, 399−414.

(6) Lourenço, S. C.; Moldão-Martins, M.; Alves, V. D. Antioxidants of Natural Plant Origins: From Sources to Food Industry Applications. *Molecules* **2019**, *24*, 4132−4157.

(7) Valgimigli, L.; Baschieri, A.; Amorati, R. Antioxidant Activity of Nanomaterials. *J. Mater. Chem. B* **2018**, *6* (14), 2036−2051.

(8) Khalil, I.; Yehye, W. A.; Etxeberria, A. E.; Alhadi, A. A.; Dezfooli, S. M.; Julkapli, N. B. M.; Basirun, W. J.; Seyfoddin, A. Nano-antioxidants: Recent Trends in Antioxidant Delivery Applications. *Antioxidants* **2020**, *9* (1), 24−54.

(9) Ghorbani, M.; Derakhshankhah, H.; Jafari, S.; Salatin, S.; Dehghanian, M.; Falahati, M.; Ansari, A. Nanozyme Antioxidants as Emerging Alternatives for Natural Antioxidants: Achievements and Challenges in Perspective. *Nano Today* **2019**, *29*, 100775−100797.

(10) Baschieri, A.; Amorati, R. Methods to Determine Chain-Breaking Antioxidant Activity of Nanomaterials beyond DPPH•. A Review. *Antioxidants* **2021**, *10* (10), 1551−1572.

(11) Lord, M. S.; Berret, J. F.; Singh, S.; Vinu, A.; Karakoti, A. S. Redox Active Cerium Oxide Nanoparticles: Current Status and Burning Issues. *Small* **2021**, *17* (51), No. 2102342.

(12) Dhall, A.; Self, W. Cerium Oxide Nanoparticles: A Brief Review of Their Synthesis Methods and Biomedical Applications. *Antioxidants* **2018**, *7*, 97−110.

(13) Heckert, E. G.; Karakoti, A. S.; Seal, S.; Self, W. T. The Role of Cerium Redox State in the SOD Mimetic Activity of Nanoceria. *Biomaterials* **2008**, *29* (18), 2705−2709.

(14) Li, F.; Yang, L.; Zou, L.; Wu, Y.; Hu, C.; He, J.; Yang, X. Decreasing Crystallinity Is Beneficial to the Superoxide Dismutase-like Activity of Ceria Nanoparticles. *ChemNanoMat* **2022**, *8* (3), No. e202100466.

(15) Lee, S. S.; Song, W.; Cho, M.; Puppala, H. L.; Nguyen, P.; Zhu, H.; Segatori, L.; Colvin, V. L. Antioxidant Properties of Cerium Oxide Nanocrystals as a Function of Nanocrystal Diameter and Surface Coating. *ACS Nano* **2013**, *7* (11), 9693−9703.

(16) Sozarukova, M. M.; Shestakova, M. A.; Teplonogova, M. A.; Izmailov, D. Y.; Proskurnina, E. V.; Ivanov, V. K. Quantification of Free Radical Scavenging Properties and SOD-Like Activity of Cerium Dioxide Nanoparticles in Biochemical Models. *Russ. J. Inorg. Chem.* **2020**, *65* (4), 597−605.

(17) Agarwal, R. G.; Kim, H. J.; Mayer, J. M. Nanoparticle O-H Bond Dissociation Free Energies from Equilibrium Measurements of Cerium Oxide Colloids. *J. Am. Chem. Soc.* **2021**, *143* (7), 2896−2907.

(18) Schrauben, J. N.; Hayoun, R.; Valdez, C. N.; Braten, M.; Fridley, L.; Mayer, J. M. Titanium and Zinc Oxide Nanoparticles Are Proton-Coupled Electron Transfer Agents. *Science* **2012**, *336* (6086), 1298−1301.

(19) Peper, J. L.; Gentry, N. E.; Boudy, B.; Mayer, J. M. Aqueous TiO2Nanoparticles React by Proton-Coupled Electron Transfer. *Inorg. Chem.* **2022**, *61* (2), 767−777.

(20) Ghosh, S.; Castillo-Lora, J.; Soudackov, A. V.; Mayer, J. M.; Hammes-Schiffer, S. Theoretical Insights into Proton-Coupled Electron Transfer from a Photoreduced ZnO Nanocrystal to an Organic Radical. *Nano Lett.* **2017**, *17* (9), 5762−5767.

(21) Warburton, R. E.; Mayer, J. M.; Hammes-Schiffer, S. Proton-Coupled Defects Impact O-H Bond Dissociation Free Energies on Metal Oxide Surfaces. *J. Phys. Chem. Lett.* **2021**, *12* (40), 9761−9767.

(22) Challa, S. S. R. K. Nanoporous Cerium Oxide Nanoparticle Macro-Structure. US Patent US17/390,199, 2022.

(23) Nikolova, M. P.; Chavali, M. S. Metal Oxide Nanoparticles as Biomedical Materials. *Biomimetics* **2020**, *5*, 27−74.

(24) Baschieri, A.; Zongxin, J.; Amorati, R. Hydroperoxyl radical (HOO•) as a reducing agent: unexpected synergy with antioxidants. A review. *Free Radical Res.* **2023**, *57*, 115−129.
(25) Cedrowski, J.; Litwinienko, G.; Baschieri, A.; Amorati, R. Hydroperoxyl Radicals (HOO•): Vitamin E Regeneration and H-Bond Effects on the Hydrogen Atom Transfer. *Chem. - Eur. J.* **2016**, *22* (46), 16441−16445.
(26) Poon, J. F.; Zilka, O.; Pratt, D. A. Potent Ferroptosis Inhibitors Can Catalyze the Cross-Dismutation of Phospholipid-Derived Peroxyl Radicals and Hydroperoxyl Radicals. *J. Am. Chem. Soc.* **2020**, *142* (33), 14331−14342.
(27) Baschieri, A.; Valgimigli, L.; Gabbanini, S.; Dilabio, G. A.; Romero-Montalvo, E.; Amorati, R. Extremely Fast Hydrogen Atom Transfer between Nitroxides and HOO• Radicals and Implication for Catalytic Coantioxidant Systems. *J. Am. Chem. Soc.* **2018**, *140* (32), 10354−10362.
(28) Harrison, K. A.; Haidasz, E. A.; Griesser, M.; Pratt, D. A. Inhibition of Hydrocarbon Autoxidation by Nitroxide-Catalyzed Cross-Dismutation of Hydroperoxyl and Alkylperoxyl Radicals. *Chem. Sci.* **2018**, *9* (28), 6068−6079.
(29) Guo, Y.; Baschieri, A.; Amorati, R.; Valgimigli, L. Synergic Antioxidant Activity of γ-Terpinene with Phenols and Polyphenols Enabled by Hydroperoxyl Radicals. *Food Chem.* **2021**, *345*, No. 128468.
(30) Guo, Y.; Baschieri, A.; Mollica, F.; Valgimigli, L.; Cedrowski, J.; Litwinienko, G.; Amorati, R. Hydrogen Atom Transfer from HOO• to Ortho-Quinones Explains the Antioxidant Activity of Polydopamine. *Angew. Chem., Int. Ed.* **2021**, *60* (28), 15220−15224.
(31) Ma, R.; Islam, M. J.; Reddy, D. A.; Kim, T. K. Transformation of CeO2 into a Mixed Phase CeO2/Ce2O3 Nanohybrid by Liquid Phase Pulsed Laser Ablation for Enhanced Photocatalytic Activity through Z-Scheme Pattern. *Ceram. Int.* **2016**, *42* (16), 18495−18502, DOI: 10.1016/j.ceramint.2016.08.186.
(32) Cerium | XPS Periodic Table | Thermo Fisher Scientific - US. https://www.thermofisher.com/us/en/home/materials-science/learning-center/periodic-table/lanthanide-rare-earth/cerium.htmlhttps://www.thermofisher.com/us/en/home/materials-science/learning-center/periodic-table/lanthanide-rare-earth/cerium.html. (accessed February 08, 2023).
(33) Vicario, G.; Balducci, G.; Fabris, S.; De Gironcoli, S.; Baroni, S. Interaction of Hydrogen with Cerium Oxide Surfaces: A Quantum Mechanical Computational Study. *J. Phys. Chem. B* **2006**, *110* (39), 19380−19385.
(34) Castillo-Lora, J.; Delley, M. F.; Laga, S. M.; Mayer, J. M. Two-Electron-Two-Proton Transfer from Colloidal ZnO and TiO2Nanoparticles to Molecular Substrates. *J. Phys. Chem. Lett.* **2020**, *11* (18), 7687−7691.
(35) Warren, J. J.; Tronic, T. A.; Mayer, J. M. Thermochemistry of Proton-Coupled Electron Transfer Reagents and Its Implications. *Chem. Rev.* **2010**, *110* (12), 6961−7001.
(36) Agarwal, R. G.; Wise, C. F.; Warren, J. J.; Mayer, J. M. Correction to Thermochemistry of Proton-Coupled Electron Transfer Reagents and Its Implications. *Chem. Rev.* **2010**, *110* (12), 6961−7001.
(37) Tan, Z.; Li, G.; Chou, H. L.; Li, Y.; Yi, X.; Mahadi, A. H.; Zheng, A.; Edman Tsang, S. C.; Peng, Y. K. Differentiating Surface Ce Species among CeO2 Facets by Solid-State NMR for Catalytic Correlation. *ACS Catal.* **2020**, *10* (7), 4003−4011.
(38) Zhang, Y.; Zhou, K.; Zhai, Y.; Qin, F.; Pan, L.; Yao, X. Crystal Plane Effects of Nano-CeO_2 on Its Antioxidant Activity. *RSC Adv.* **2014**, *4*, 50325−50330.
(39) Yang, Y.; Mao, Z.; Huang, W.; Liu, L.; Li, J.; Li, J.; Wu, Q. Redox Enzyme-Mimicking Activities of CeO2 Nanostructures: Intrinsic Influence of Exposed Facets. *Sci. Rep.* **2016**, *6*, No. 35344.
(40) Valgimigli, L.; Pratt, D. A. Maximizing the Reactivity of Phenolic and Aminic Radical-Trapping Antioxidants: Just Add Nitrogen! *Acc. Chem. Res.* **2015**, *48* (4), 966−975.
(41) Amorati, R.; Challa, S. S. R. K. Nanoporous Cerium Oxide Nanoparticle Macrostructures as Autooxidation Inhibitors. US Patent US17/817,858, 2022.

https://doi.org/10.1021/acsomega.3c03654
ACS Omega 2023, 8, 40174−40183